Geochemistry Geophysics Geosystems G3
AN ELECTRONIC JOURNAL OF THE EARTH SCIENCES
Published by AGU and the Geochemical Society

Article
Volume 10, Number 12
16 December 2009
Q12009, doi:10.1029/2009GC002665
ISSN: 1525-2027

Five million years of compositionally diverse, episodic volcanism: Construction of Davidson Seamount atop an abandoned spreading center

D. A. Clague and J. B. Paduan
Monterey Bay Aquarium Research Institute, 7700 Sandholdt Road, Moss Landing, California 95039, USA (clague@mbari.org)

R. A. Duncan and J. J. Huard
College of Oceanic and Atmospheric Sciences, Oregon State University, 104 COAS Administration Building, Corvallis, Oregon 97331, USA

A. S. Davis
Monterey Bay Aquarium Research Institute, 7700 Sandholdt Road, Moss Landing, California 95039, USA

P. R. Castillo and P. Lonsdale
Scripps Institution of Oceanography, University of California, San Diego, 9500 Gilman Drive, La Jolla, California 92093, USA

A. DeVogelaere
Monterey Bay National Marine Sanctuary, NOAA, 299 Foam Street, Monterey, California 93940, USA

[1] Davidson Seamount, a volcano located about 80 km off the central California coast, has a volume of ~320 km^3 and consists of a series of parallel ridges serrated with steep cones. Davidson was sampled and its morphology observed during 27 ROV *Tiburon* dives. During those dives, 286 samples of lava, volcaniclastite, and erratics from the continental margin were collected, with additional samples from one ROV-collected push core and four gravity cores. We report glass compositions for 99 samples and ^{40}Ar-^{39}Ar incremental heating age data for 20 of the samples. The glass analyses are of hawaiite (62%), mugearite (13%), alkalic basalt (9%), and tephrite (8%), with minor transitional basalt (2%), benmoreite (2%), and trachyandesite (2%). The lithologies are irregularly distributed in space and time. The volcano erupted onto crust inferred to be 20 Ma from seafloor magnetic anomalies. Ages of the lavas range from 9.8 to 14.8 Ma. The oldest rocks are from the central ridge, and the youngest are from the flanks and southern end of the edifice. The compositions of the 18 reliably dated volcanic cones vary with age such that the oldest lavas are the most fractionated. The melts lost 65% to nearly 95% of their initial S because of bubble loss during vesiculation, and the shallowest samples have S contents similar to lava erupted subaerially in Hawaii. Despite this similarity in S contents, there is scant other evidence to suggest that Davidson was ever an island. The numerous small cones of disparate chemistry and the long eruptive period suggest episodic growth of the volcano over at least 5 Myr and perhaps as long as 10 Myr if it began to grow when the spreading ridge was abandoned.

Components: 9002 words, 10 figures, 1 table.

Keywords: seamount; submarine volcano; explosive volcanism; remotely operated vehicle.

Index Terms: 8416 Volcanology: Mid-oceanic ridge processes (1032, 3614); 8150 Tectonophysics: Plate boundary: general (3040); 8178 Tectonophysics: Tectonics and magmatism.

Received 4 June 2009; **Revised** 17 July 2009; **Accepted** 15 September 2009; **Published** 16 December 2009.

Clague, D. A., J. B. Paduan, R. A. Duncan, J. J. Huard, A. S. Davis, P. R. Castillo, P. Lonsdale, and A. DeVogelaere (2009), Five million years of compositionally diverse, episodic volcanism: Construction of Davidson Seamount atop an abandoned spreading center, *Geochem. Geophys. Geosyst.*, *10*, Q12009, doi:10.1029/2009GC002665.

1. Introduction

[2] Davidson Seamount is one of nine seamounts off the continental margin of the southwestern U.S. and several more off Baja, Mexico built on or near axes of the East Pacific Rise (Figure 1) that ceased spreading in the Miocene. They are unrelated to a subduction arc, unassociated with identified active mid-ocean ridges, and not parts of linear volcanic chains. These seamounts have steep, linear morphology, and diverse chemistry and ages. Their sporadic, small-volume, explosive eruptions were roughly synchronous at widely scattered locations [*Davis et al.*, 1995, 2002]. They erupted onto the seafloor along existing fractures and zones of weakness in the tectonic plate due to decompression melting of the mantle below [*Davis et al.*, 2002; P. Castillo et al., Petrogenesis of Davidson Seamount lavas and its implications for fossil spreading center and intraplate magmatism in the eastern Pacific, submitted to *Geochemistry, Geophysics, Geosystems*, 2009]. The formation of Davidson, and other similar seamounts at sites of abandoned spreading centers, may be caused by transient upwelling of the mantle directly beneath fossil spreading centers due to buoyancy driven by its thermal and/or compositional difference with the surrounding mantle (Castillo et al., submitted manuscript, 2009). The unusual large size of some of these ridges, including Davidson Seamount, offshore western North America may also be related to transtensional forces near the continental margin that allow volcanism to continue long after spreading ceased (A. S. Davis et al., Origin of volcanic seamounts offshore California related to interaction of abandoned spreading centers with the continental margin, manuscript in preparation, 2009).

[3] Davidson Seamount was the first underwater mountain to be named a seamount, and is the most thoroughly studied of the seamounts along the western U.S. Davidson is about 42 km long and only 13.5 km wide and rises 2400 m from the seafloor to its summit at 1256 m, as mapped by the *MBARI Mapping Team* [2001]. Its volume is about 320 km^3. There is a low-relief pedestal surrounding the seamount, particularly on the southeast side that apparently also postdates the underlying seafloor. Davidson has been explored with dredging by the USGS [*Davis et al.*, 2002; *Davis and Clague*, 2003], 30 kHz multibeam sonar mapping in 1998 [*MBARI Mapping Team*, 2001], 200 kHz multibeam sonar mapping of part of the seamount conducted in 2006 by the MBARI AUV *D. Allan B.*, and 27 ROV *Tiburon* dives in 2000, 2002, 2006, and 2007. The dives in 2000, funded by the National Undersea Research Program (NURP) and MBARI, were primarily focused on the geology of the seamount. The subsequent dives have mainly been conducted on expeditions led by NOAA's Monterey Bay National Marine Sanctuary (MBNMS) with funding from the Ocean Exploration Program and the British Broadcasting Corporation which were primarily interested in the fauna on the seamount, particularly the large corals that inhabit the summits [*Andrews et al.*, 2005]. The seamount has been added to the MBNMS, primarily to protect the large coral communities and fragile ecosystem [*DeVogelaere et al.*, 2005]. The numerous dives on Davidson have fostered studies of the benthic invertebrate communities [*Lundsten et al.*, 2009a] and ichthyfauna [*Lundsten et al.*, 2009b].

[4] Lava petrography, glass chemistry and Ar-Ar ages of the lavas collected during all the ROV *Tiburon* dives are presented here. Whole-rock trace element and radiogenic isotopic data and a detailed petrogenesis of the lavas are presented by Castillo et al. (submitted manuscript, 2009), and a geologic analysis of the high-resolution AUV mapping data and visual observations from the dives are presented by J. B. Paduan et al. (High-resolution multibeam and visual mapping of Davidson Seamount, manuscript in preparation, 2009).

2. Geologic Setting and Previous Work

[5] Davidson Seamount is located 80 km west of Big Sur, California (Figure 2). It is a ridge about

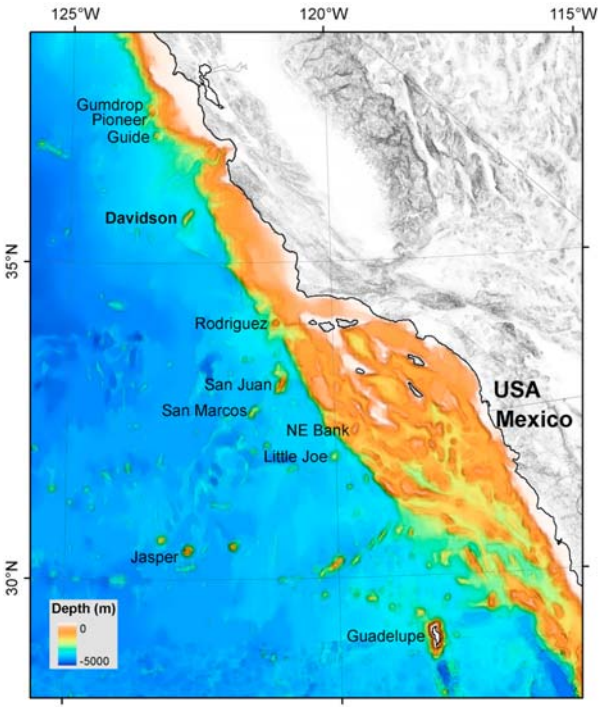

Figure 1. Regional bathymetric UTM map showing the location of Davidson Seamount offshore central California. Other related and nearby seamounts are identified with the seamount and island names placed just west of the features.

42 km long and 13.5 km wide and rises about 2400 m to 1250 m depth and has a volume above the seafloor of about 320 km^3 [*Davis et al.*, 2002]. It also lies along the axis of symmetry of northeast striking magnetic stripes C6AAr,2n to C6n, implying that it overlies an abandoned spreading center that ceased spreading between 20 and 18 Ma, after accreting crust between the Pacific and Monterey microplate at a rate of 45 mm/yr for the preceding 2.5 Ma (Figure 2) [*Atwater and Severinghaus*, 1989; after *Lonsdale*, 1991]. Many of the other seamounts off the continental margin of the western U.S. and Mexico are located roughly parallel to abandoned spreading centers as are Guadalupe Island [*Batiza*, 1977], the Mathematician Ridge [*Bohrson et al.*, 1996], a number of volcanic ridges offshore Baja California [*Lonsdale*, 1991; *Tian et al.*, 2008] in the eastern Pacific, and an axial seamount in the Antarctic-Phoenix Ridge in the Drake Passage between South America and Antarctica [*Choe et al.*, 2007; *Choi et al.*, 2008]. All are examples of seamounts clearly located at the site of an abandoned spreading center. In the eastern Pacific, the remainder of the seamounts are oriented parallel to magnetic anomalies, but do not have symmetric magnetic anomalies adjacent to the seamount. The southwest end of Davidson abuts the Morro Fracture Zone, a fossil transform fault [*Lonsdale*, 1991].

[6] Three superficial rocks dredged from Davidson were previously dated at 12.16 ± 0.43 Ma [*Davis et al.*, 2002] showing that Davidson continued to erupt for several Ma after spreading ceased. A fourth sample, dated at 16.75 ± 0.10 Ma, is an andesite now inferred to be an erratic [*Davis et al.*, 2002; *Paduan et al.*, 2007].

[7] Ten analyzed dredged whole-rock samples and 9 analyzed glasses [*Davis et al.*, 2002] range from alkalic basalt to mugearite in composition, similar to the lavas from other seamounts off the continental margin of the western U.S. [*Davis et al.*, 2002, also manuscript in preparation, 2009]. The isotopic compositions are mostly MORB-like but variable, indicating they were generated from a depleted mantle source but with variable enrichment [*Davis et al.*, 2002, also manuscript in preparation, 2009; Castillo et al., submitted manuscript, 2009]. All of the alkalic samples are highly vesicular [*Davis et al.*, 2002] and volcaniclastic rocks of submarine pyroclastic origin are common in the dredged and ROV collected samples [*Davis and Clague*, 2003]. The lavas and volcaniclastic rocks contain a variety of ultramafic and mafic xenoliths and xenocrysts that represent the upper mantle beneath the seamount and cumulates of the ocean crust and deep magma reservoirs associated with the volcano [*Davis et al.*, 2007].

3. Methods

[8] Davidson has been mapped with 30 kHz EM300 multibeam sonar [*MBARI Mapping Team*, 2001] and the surrounding region mapped at lower frequencies, yielding maps of 20 m resolution for the summit and flanks, and 40 m resolution for the base of the seamount. Portions of the summit and SW ridge were mapped with near-bottom 200 kHz multibeam sonar using MBARI's Mapping AUV for five missions in 2006. The terrain proved highly challenging to survey due to steep slopes. The data are presented and interpreted with visual observations of the geology of the bottom in the work by Paduan et al. (manuscript in preparation, 2009).

[9] Twenty-seven successful ROV *Tiburon* dives completed in 2000 (8 dives T139–T147), 2002 (6 dives T425 to T430), 2006 (12 dives T939 to T951 and T1064), and 2007 (dive T1102) are shown on a bathymetric map of Davidson in Figure 1. Geologic sampling and observations were the pri-

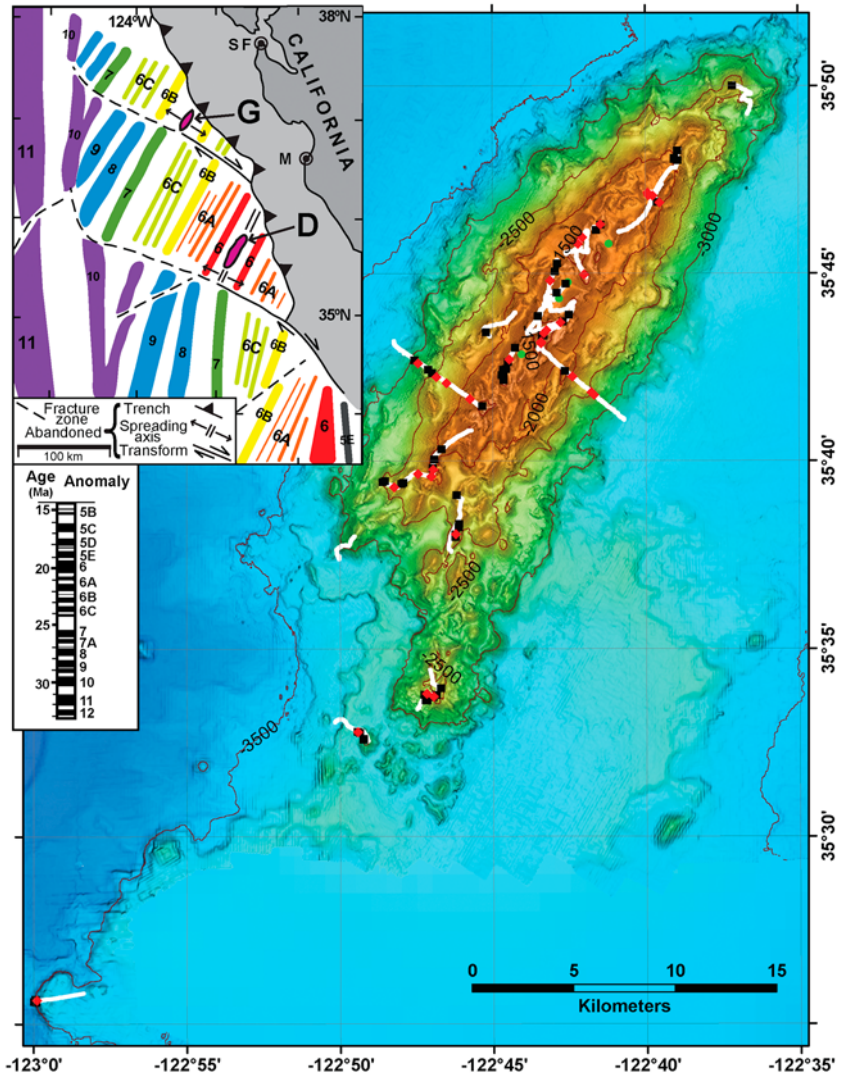

Figure 2. Multibeam bathymetric map of Davidson Seamount showing the locations of 27 ROV dives completed since 2000 (white lines). All 27 dives recorded observations useful for geologic mapping, and rock samples were collected on 20 of the dives. The colored symbols show the locations of the glasses presented here, divided into lava rinds, volcaniclastic rocks, and gravels (unconsolidated volcaniclastic rocks). Inset shows the locations of spreading axis seamounts Davidson (D) and Guide (G), relative to the California coast (SF, San Francisco; M, Monterey) and to the pattern of magnetic stripes on oceanic crust [after *Lonsdale*, 1991], and shows that Davidson is bounded by anomaly 6 of both sides and that the seamount is located atop a ridge crest abandoned about 20 Ma.

mary objectives of only 8 dives (T139–T142 and T144–T147) in 2000, with ecology of benthic fauna or collection of underwater video for broadcast purposes the primary objectives of 18 others in 2002 and 2006. The primary objective of the one remaining dive (T1102) in 2007 was to collect bamboo corals for paleoceanographic study.

[10] Navigation of the ROV employs an ultrashort-baseline (USBL) system with data recorded for onshore processing. For the dives in 2000, a problem in the recording system led to loss of this real-time data stream. However, positions fit by eye to the many positions at sea were recorded as a mark point file in a real-time navigation system operated in a Geographic Information System (GIS). The navigation for these dives was reconstructed from these mark point files by linearly interpolating positions between mark points. The first dive in 2002 (T425) was run with no USBL navigation and the track of this dive has been reconstructed using a known start and end point (where a fish trap and Homer beacon were deployed and then recovered on a subsequent dive, providing a location for the start and end location for dive T425). The relative track during the dive

was determined by the Doppler Velocimeter Log on the ROV and then further adjusted so that the bathymetry along the dive track matched the underlying bathymetry of the seamount. The dive track and sample locations (two rock samples) are more uncertain for this dive than for the others.

[11] Table S1 in the auxiliary material lists each analyzed collected sample, analyses performed, lithology (lava flow or volcaniclastite), rock classification (e.g., alkalic basalt, hawaiite, mugearite, etc.), depth of collection, location (latitude and longitude in decimal degrees), and references to all analyses for each sample.[1]

[12] Samples were collected with the ROV's manipulator arm and push cores. During the 2007 program, we deployed a gravity corer into sediment ponds located between cones. The first 2 cores were empty, but the next four recovered small amounts of sand and gravel. Polished thin section for 99 samples with fresh glass from glass rinds (62 samples), volcaniclastic breccia (32 samples), or volcanic gravel recovered in the 4 gravity cores (S07GC3 to 6) and one push core (T1102PC56), were analyzed with a JEOL 8900 Superprobe at the USGS in Menlo Park. Analyses were performed with 15 kv accelerating voltage, 20 nAmps specimen current, using a 50 μm beam size and natural and synthetic glass and mineral standards [e.g., *Davis et al.*, 1994]. Each analysis is typically the average of five or more points. Smithsonian glass standard VG-2 was used as the internal standard for Si, Al, Fe, Mg, Ca, and Na and standards A99 and VG2 were used to monitor for instrument drift. Three of these host glasses were analyzed for volatile components by ion probe [see *Davis and Clague*, 2003, Table 3]. An additional 9 glass analyses of hawaiite and mugearite and 7 whole-rock major and trace element analyses of dredged alkalic basalt, hawaiite and mugearite samples are presented by *Davis et al.* [2002].

[13] Fourteen glass inclusions and their host mineral phases were analyzed using the same conditions and standards, but using a focused beam, but each analysis is a single point analysis. We analyzed only a single olivine crystal with an unaltered glass inclusion, but we found a number of large clinopyroxene crystals with trapped fresh glass inside. These clinopyroxene crystals were recovered as loose gravel in two gravity cores. Additional analyses of phenocrysts and microphenocrysts of olivine, clinopyroxene, and plagioclase from a subset of these samples and some dredged samples described by *Davis and Clague* [2003] are given by *Davis et al.* [2007, supplemental materials].

[14] Based on thin section examination, 20 samples were selected for radiometric dating. For 4 samples with abundant, unaltered plagioclase, and two additional samples containing biotite or amphibole, the age measurements were performed on acid-treated mineral separates, using techniques described by *Koppers et al.* [2000]. For sparsely phyric or aphyric samples, age determinations were made on either crystalline groundmass separates (4 samples) or on minicores of the least altered part of whole rocks (9 samples), following methods described by *Duncan and Keller* [2004]. Mineral separates and crystalline groundmass separates were analyzed using a 10 W CO_2 continuous laser probe [*Koppers et al.*, 2003] and whole rock disks by incremental heating with a double-vacuum resistance furnace [*Duncan and Keller*, 2004]. All samples were irradiated in Oregon State University's IMW TRIGA reactor for 6 h, using the flux monitor standard 28.04 Ma old FCT-3 biotite [*Renne et al.*, 1998]. Details of the irradiation, calibration, and age calculations are described by *Koppers et al.* [2003]. Age plateaus and isochrons were calculated using software described by *Koppers* [2002].

4. Results

4.1. The ^{40}Ar-^{39}Ar Age Data

[15] These samples yielded excellent ^{40}Ar-^{39}Ar incremental heating data, probably because of the high K_2O contents, minimal groundmass alteration, and our ability to separate clean mineral separates in some cases. We prefer the plateau ages as the most representative of the ages of the samples and use those ages throughout the paper. The age data summarized in Table 1 show that the plateau ages range from 9.77 ± 0.15 Ma to 14.83 ± 0.18 Ma. Complete data for each sample are posted at http://www.mbari.org/volcanism/Seamounts/Default.htm.

[16] Of the 20 samples dated, whole-rock sample T146R11 yielded no plateau and no usable inverse isochron, but amphibole separated from the same rock yielded consistent plateau, inverse isochron, and total fusion ages with a plateau age of 12.77 ± 0.27 Ma. Sample T147R9 yielded identical ages of 12.56 ± 0.15 Ma for separated biotite and 12.76 ± 0.23 for the whole-rock. For subsequent plots, we use the mineral plateau ages for these two samples.

[1] Auxiliary materials are available at ftp://ftp.agu.org/apend/gc/2009gc002665.

Table 1. Summary of $^{40}Ar/^{39}Ar$ Radiometric Age Determinations[a]

Sample	Material	Lab Number	Plateau (Ma)				Inverse Isochron (Ma)		Total Fusion Age ± 2σ
			Age ± 2σ	Steps	% ^{39}Ar	MSWD	Age ± 2σ	$^{40}Ar/^{36}Ar$ ± 2σ	
T140R14	whole rock	02C639	**14.19 ± 0.13**	3/8	59	0.78	**14.24 ± 0.17**	270.6 ± 44.8	**14.03 ± 0.13**
T141R3	whole rock	02C630	**11.88 ± 0.17**	3/9	55.1	0.48	**11.92 ± 0.20**	281.9 ± 38.5	11.07 ± 0.15
T141R18	whole rock	02C656	**14.83 ± 0.16**	4/8	68.7	0.29	**14.84 ± 0.17**	294.6 ± 5.8	13.46 ± 0.14
T142R9	whole rock	02C618	**14.38 ± 0.18**	5/11	47.4	0.14	**14.40 ± 0.20**	292.1 ± 17.7	13.47 ± 0.16
T142R22	whole rock	02C677	**14.23 ± 0.22**	6/8	81.7	0.82	**14.23 ± 0.23**	295.7 ± 3.2	**14.00 ± 0.23**
T144R13	whole rock	O2C609	**9.77 ± 0.15**	3/9	17.8	2.22	**9.51 ± 0.30**	325.0 ± 30.7	8.73 ± 0.10
T145R1	whole rock	02C588	**10.30 ± 0.15**	5/9	71.7	1.34	**10.29 ± 0.16**	298.9 ± 9.9	**10.01 ± 0.15**
T145R10	whole rock	02C574	**11.17 ± 0.25**	3/7	67.9	2.49	**11.07 ± 0.78**	297.4 ± 13.9	9.83 ± 0.23
T146R11	amphibole	02C664	**12.77 ± 0.27**	3/5	99.3	0.2	**12.73 ± 0.33**	314.5 ± 87.6	**12.87 ± 0.30**
T146R11	whole rock	02C669	no plateau				no isochron		12.14 ± 0.15
T147R9	biotite	02C581	**12.56 ± 0.15**	6/7	99.8	0.32	**12.57 ± 0.15**	294.5 ± 7.9	**12.56 ± 0.15**
T147R9	whole rock	02C647	**12.76 ± 0.23**	4/9	42	14.98	13.43 ± 0.34	176.2 ± 49.1	**12.42 ± 0.17**
T426R13	plagioclase	04C3473	**11.57 ± 0.16**	5/7	87.8	2.15	**11.61 ± 0.19**	281.0 ± 33.9	**11.78 ± 0.14**
T427R5	groundmass	05C436	**10.92 ± 0.16**	2/7	59.4	1.79	no isochron		**10.92 ± 0.13**
T428R4	groundmass	05C443	**12.20 ± 0.14**	4/8	68.9	0.47	**12.20 ± 0.15**	295.5 ± 6.3	11.78 ± 0.18
T429R7	plagioclase	05C471	**14.68 ± 0.22**	4/7	59.1	0.34	**14.78 ± 0.29**	266.4 ± 57.6	16.00 ± 0.21
T429R24	groundmass	05C451	**14.75 ± 0.14**	9/10	98.7	2.19	**14.74 ± 0.15**	297.3 ± 8.8	**14.80 ± 0.13**
T430R4	plagioclase	04C3466	**13.84 ± 0.26**	5/7	91.4	0.91	**13.88 ± 0.30**	292.8 ± 9.2	14.87 ± 0.28
T430R22	groundmass	05C461	**12.82 ± 0.17**	4/9	64.5	2.94	**12.93 ± 0.18**	284.0 ± 11.9	12.06 ± 0.13
T1102R7	plagioclase	08C429	**11.60 ± 0.05**	10/14	56.0	2.53	**11.66 ± 0.10**	281.0 ± 23.8	11.12 ± 0.05

[a] Ages calculated using biotite monitor FCT-3 (28.04 Ma) and total decay constant l = 5.530E-10/yr. Steps are the number of heating steps (defining plateau/total); MSWD is an F statistic that compares the variance within step ages with the variance about the plateau age. Ages in bold are concordant plateau, isochron, and total fusion ages.

Groundmass sample T427R5 yielded no useful inverse isochron, but the plateau age and total fusion age are the same at 10.92 Ma. The plateau ages and inverse isochron ages of the other 18 samples are statistically identical. Of those, ten did not yield statistically identical total fusion ages but only two yielded total fusion ages older than the plateau and isochron ages, with all the others too young. The plateau age of the one sample with no isochron is statistically indistinguishable from the total fusion age.

[17] The ages of the 18 different dated volcanic cones are not evenly spaced in time, with 6 cones dated between 14 and 15 Ma, only one between 13 and 14 Ma, 4 between 12 and 13 Ma, 4 between 11 and 12 Ma, 2 between 10 and 11 Ma, and only one younger than 10 Ma. There is a general trend of decreasing activity through the 5 Ma of volcanic history documented on Davidson.

[18] The ages of the samples follow no systematic spatial pattern (Figure 3), with older and younger samples scattered over the seamount. The youngest sample (T144R13) is the southernmost dated sample and also on SE periphery of the volcano, and several of the oldest samples are located near the summit of Davidson. There is no relationship between age and eruption depth (Figure 4).

[19] The ages of the samples are related to the chemistry of the rocks, although we have to compare ages to whole-rock chemistry (Castillo et al., submitted manuscript, 2009) as only two of the dated samples have glass rinds. A plot of age versus whole-rock MgO content (Figure 5) shows that the older samples are generally the most fractionated and the younger samples the least.

4.2. Glass Chemistry

[20] The glass analyses (Data Set S1), subdivided into glass lava rinds and glasses in volcaniclastic rocks or as loose gravel, are shown plotted on an alkali-silica diagram in Figure 6, with boundaries to define the rock types after *Cox et al.* [1979]. The glasses show a wide compositional variation with no obvious differences between those that form quench rinds on lava fragments and those in clastic rocks. The glasses include transitional basalt (1), alkalic basalt (8), hawaiite (62), mugearite (13), benmoreiite (2), tephrite (8), and trachyandesite (3). Clearly, most compositions are hawaiite, with less common more or less fractionated compositions. The single transitional basalt (T145R4a) contains 0.81 wt % K_2O and plots on the field boundary between alkalic and tholeiitic basalt. The range of glass compositions is slightly more restricted than the whole-rock compositions (Castillo

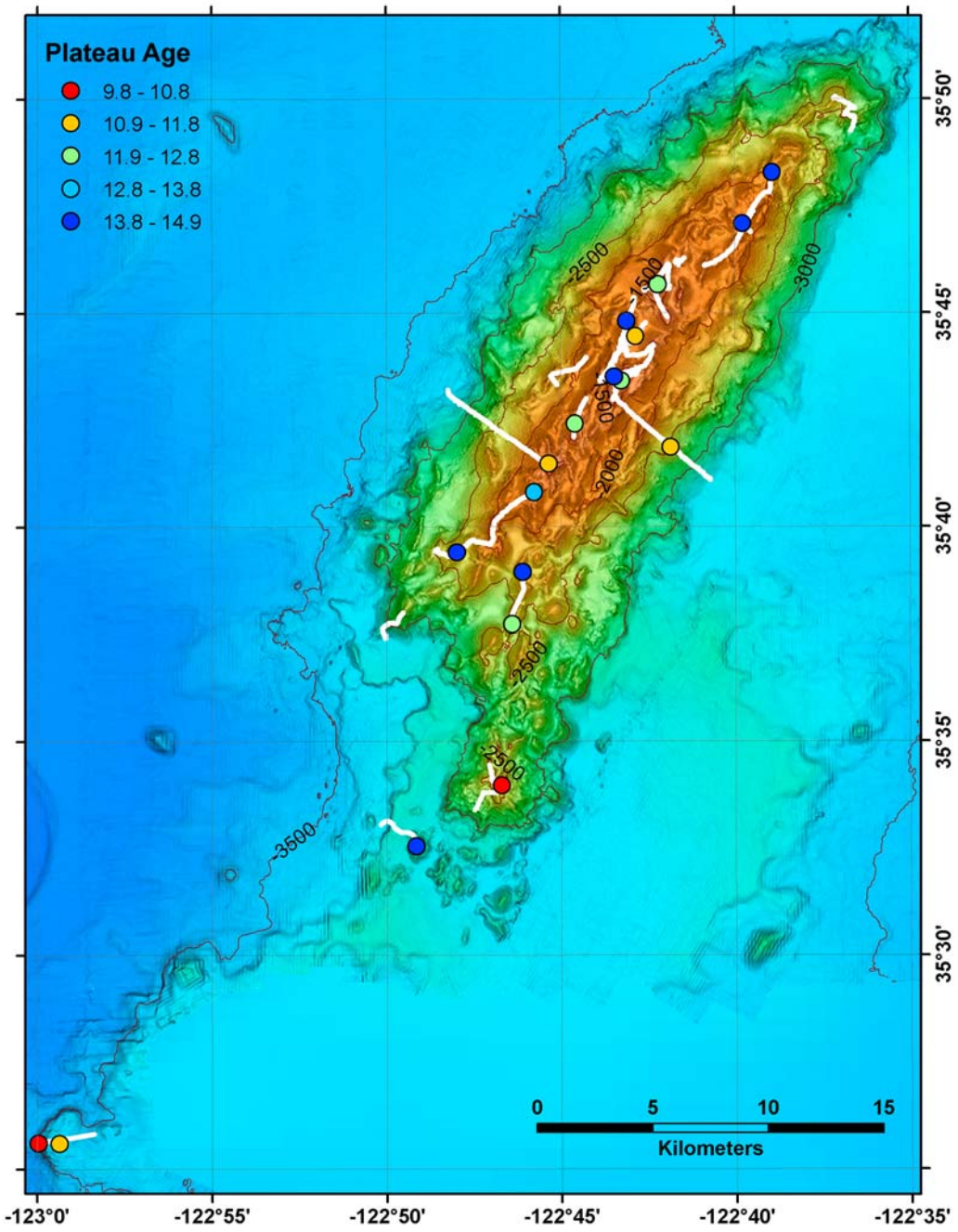

Figure 3. Multibeam bathymetric map showing plateau ages of samples determined by ^{40}Ar-^{39}Ar incremental heating, symbolized by age. No spatial organization of ages is apparent.

et al., submitted manuscript, 2009) mainly because the most fractionated trachytic lavas had no glass rinds.

[21] We have not included two analyses (T429R2 and T429R5) in Data Set S1 or plotted them in any figures. These analyses plot in the tholeiitic field, but have high K_2O (2.44 and 2.47 wt %) and P_2O_5 (0.90 and 0.92 wt %), and otherwise resemble hawaiite, except for their unusually low Na_2O (1.64 and 1.72 wt %) that shifts them into the tholeiitic field. The vesicular glasses are translucent, light brown in color, and do not appear to be altered or leached, but the abundant microlites in the glass led to use of a focused beam on the electron microprobe to avoid overlap with crystals. Their classification as tholeiitic basalt is caused by vaporization of Na_2O from the glass due to the use of the focused beam.

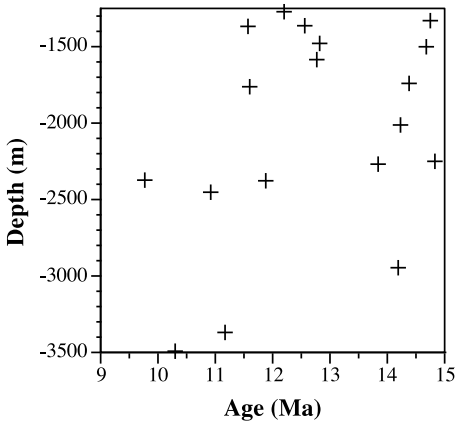

Figure 4. Depth plotted against age for 18 dated cones shows no correlation.

[22] The glass data, shown plotted on a series of MgO variation diagrams (Figure 7), show no difference between glass lava rinds and glass in volcaniclastic samples. The glasses are all strongly fractionated with only a single glass analysis having >6% MgO. With decreasing MgO, CaO decreases and the incompatible elements K_2O, P_2O_5, and Cl increase. Al_2O_3 and TiO_2 have broad increasing trends as MgO decreases from 7 to 3%. At MgO < 3%, SiO_2 also increases, and FeO, CaO, TiO_2 and P_2O_5 decrease. The glass compositions do not define coherent trends and the variations for all elements fall outside analytical uncertainties. Each glass is distinctive with wide ranges in incompatible element concentrations (K_2O, P_2O_5, and Cl) at similar MgO contents.

[23] The glass inclusion data are also plotted in Figure 7 and are not distinctive, except that their S contents extend to 0.21 wt % (2100 ppm) compared with the other glass samples with S < 0.084 wt % (840 ppm). The glass inclusions are also among the least fractionated melts (highest MgO) recovered from Davidson.

[24] The glass data for SiO_2, MgO, K_2O, and S are shown by location in Figure 8. There are no strong spatial relations in terms of silica content (Figure 8a), fractionation (MgO) (Figure 8b), or enrichment in incompatible elements (K_2O) (Figure 8c). Most, but not all, of the samples with the lowest K_2O contents (red and yellow in Figure 8c) occur deep, including those from dive T145 to the southwest of the image. On the other hand, samples with lower S contents (red and yellow in Figure 8d) are concentrated near the summit (Figure 8d) and those with higher S are generally found at greater depths on the northwestern flank and southern half of the volcano. A plot of MgO versus depth (Figure 9a) shows a subtle correlation with higher MgO glasses at greater depth, but the apparent trend is controlled by a few high-MgO glasses from deep and a few low-MgO glasses from shallow depths. A plot of S content versus depth (Figures 9b and 9c), on the other hand, shows a strong correlation with S content increasing with depth and that all the host glasses have lower S than many of the glass inclusions. A similar plot for only 12 samples [*Davis and Clague*, 2003] shows this same increase in S with increasing depth, but also shows the wide variation in S (several hundred ppm) in different clasts from single volcaniclastic samples. The lowest S contents of the glasses (<0.025% S or <250 ppm) overlap with S contents of lavas erupted above sea level in Hawaii [e.g., *Moore and Clague*, 1987] whereas the highest S content in glass inclusions (0.21 wt %) is similar to that for alkalic lavas from Loihi Seamount [*Dixon and Clague*, 2001] or the North Arch volcanic field [*Dixon et al.*, 1997].

4.3. Petrography

[25] The most striking characteristic of the glasses is their high vesicularity, regardless of collection depth or rock type. The glass rinds on flow fragments tend to have larger vesicles, that are round or elongate parallel to flow, or can become amoeboid in shape. The scoria and lapilli in volcaniclastic rocks [*Davis and Clague*, 2003] generally contain abundant small round vesicles, although some lapilli have highly stretched vesicles and are similar to tube pumice fragments. These differences in abundance, size, and shape of vesicles are shown in glass samples in Figure 10. Many lava

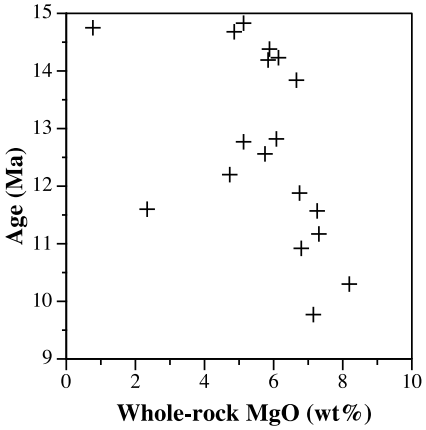

Figure 5. MgO in whole rock samples (from Castillo et al., submitted manuscript, 2009) plotted against age showing that the oldest samples are the most fractionated, lowest MgO rocks, and the youngest samples have the most primitive compositions.

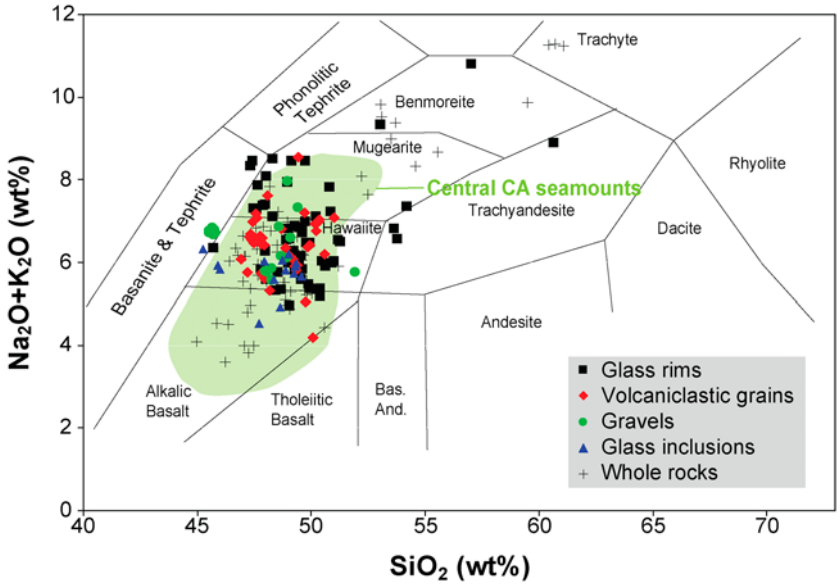

Figure 6. Alkali-SiO_2 diagram showing that most glass compositions are hawaiite but mugearite, alkalic basalt, tephrite, trachyandesite, benmoreite, and transitional basalt also occur in order of decreasing abundance. Symbols are as follows: black squares are glasses from rinds on lava flow fragments, red diamonds are glass fragments in volcaniclastic rocks, green circles are glass from loose gravel fragments recovered in cores, and blue triangles are glass inclusions in clinopyroxene and olivine crystals. Whole-rock analyses for the same sample collection from Castillo et al. (submitted manuscript, 2009) are shown as small pluses. Classification from *Cox et al.* [1979]. Green shaded field for central California seamounts is from Davis et al. (manuscript in preparation, 2009) and includes glasses from Pioneer, Guide, Gumdrop, Rodriguez, San Juan, San Marcos, and Little Joe seamounts and Northeast Bank.

samples, but only a few glass samples, contain only abundant large (>mm size) bubbles that have started to coalesce into dumbbell shaped vesicles (Figure 10a). Abundant samples of lava and glass have large spherical vesicles of nearly uniform size (Figure 10b). As the size of the largest vesicles decreases, the spherical vesicles begin to have a larger range of sizes (Figures 10c and 10d). Some of the pyroclastic samples contain fragments that have stretched bubbles, either at the edge of clasts (Figure 10e) or through entire individual small shards (Figure 10f). Bubble populations commonly exceed ~30–40% by volume, but even the fragments in volcaniclastic rocks rarely exceed ~60% bubbles.

[26] One trachyte sample (T429R24) and benmoreite samples (T425R2 and T943R2) are three of the only dense samples from Davidson. In contrast, benmorite lava samples collected from an inflated (and partially drained) lava flow (Paduan et al., manuscript in preparation, 2009) during dive T1102 (R1, R3, and R7) are slightly to moderately vesicular, as are two trachyte lavas collected on the same dive (T1102-R9 and R10), all of which have elongate stretched vesicles. Sample T145R5, a polymict basalt sandstone from 3380 m depth [*Davis and Clague*, 2003] is the only volcaniclastic sample from Davidson containing only dense glass fragments that also have two different compositions, including the sole transitional basalt recovered from Davidson (Data Set S1).

[27] The different rock types contain a range of phenocryst assemblages, although the relations are not systematic. For example, alkalic basalt glasses can contain olivine, olivine plus clinopyroxene, olivine plus plagioclase, or clinopyroxene plus plagioclase. The most common hawaiite glasses are aphyric, or contain rare olivine, olivine plus clinopyroxene (ranging to one that is an ankaramite with large clinopyroxene and smaller rare olivine), to plagioclase phyric. Less common mineral assemblages include olivine plus plagioclase, rare clinopyroxene, and olivine plus clinopyroxene plus plagioclase.

[28] Primary red-brown amphibole is present as small phenocrysts and a groundmass phase in two hawaiite glasses (T147R8 and T147R9), and two mugearite glasses (T147R8 and T147R13), all apparently from the same eruption. The glass compositions from this eruption span the boundary between hawaiite and mugearite and both are

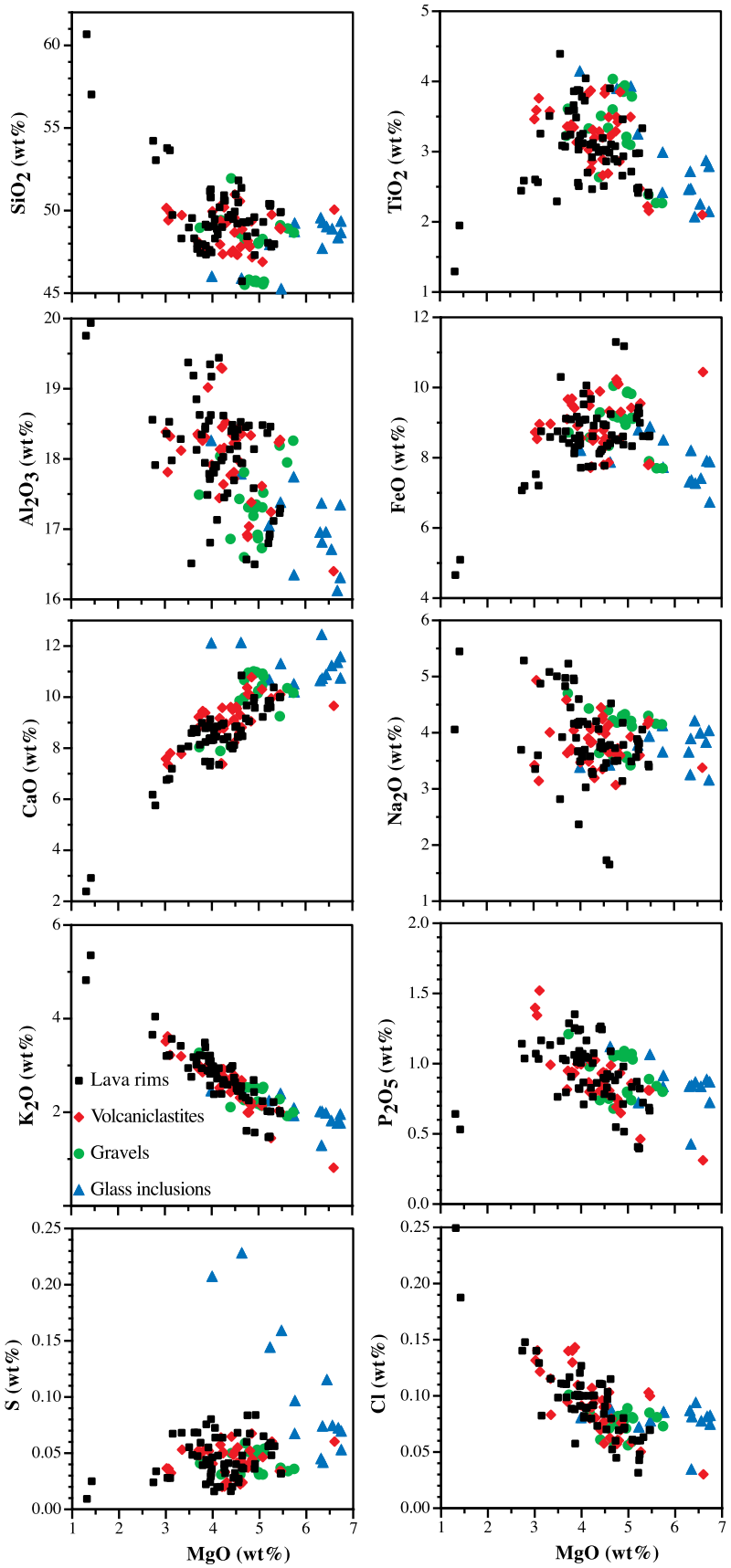

Figure 7. MgO variation diagrams showing all analyzed glass compositions. Symbols as in Figure 6.

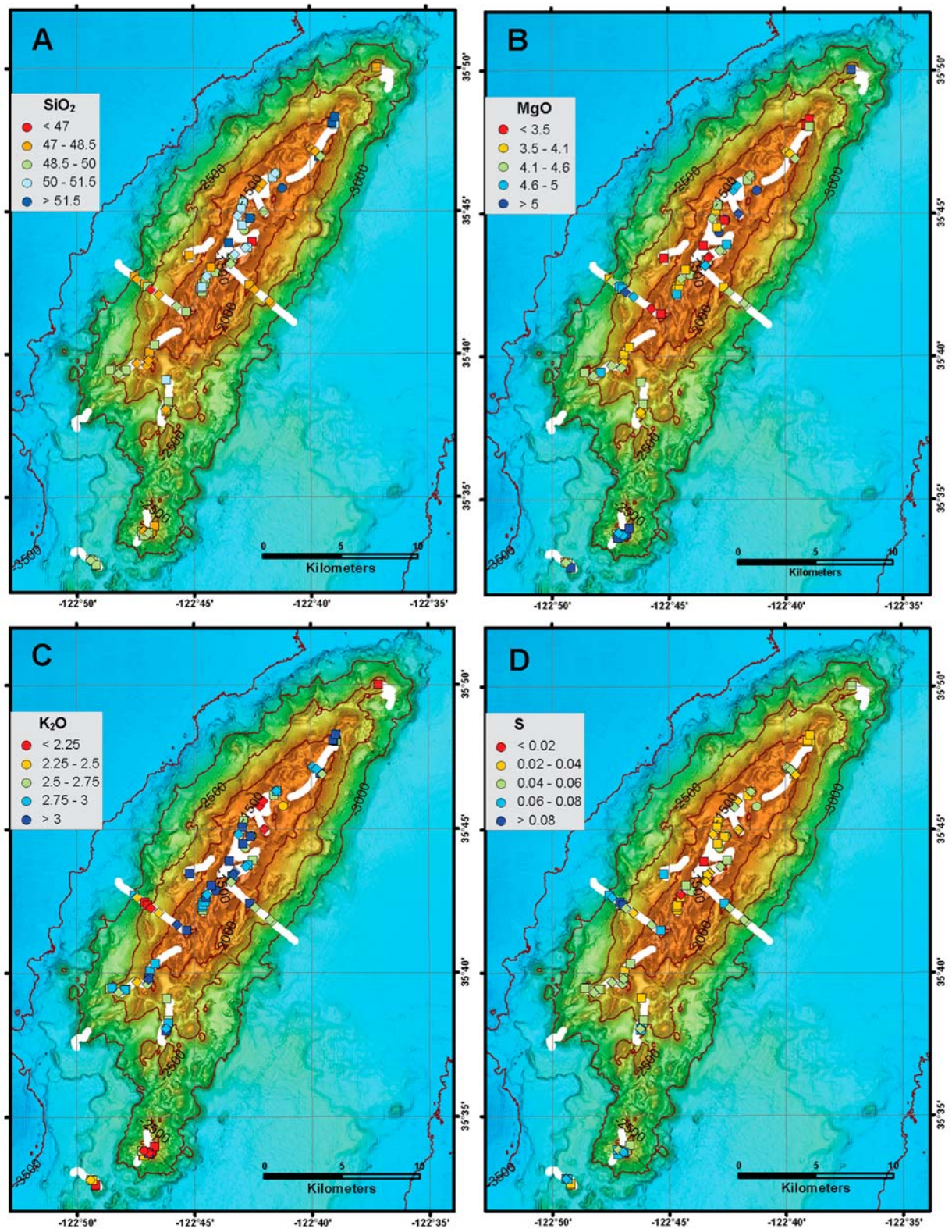

Figure 8. Multibeam bathymetric map of Davidson showing the distribution of glass compositions. Symbols as in Figure 6. (a) SiO_2 contents, (b) MgO contents, (c) K_2O content, and (d) S content. No strong spatial organization of SiO_2, MgO, or K_2O is apparent. S contents are lower in glasses from nearer the summit.

found in volcaniclastite T147R8. These are the only glasses from Davidson that contain amphibole as a primary phenocryst or groundmass phase, although numerous samples contain amphibole xenocrysts to megacrysts or xenoliths containing amphibole [*Davis et al.*, 2007]. Trachyte samples from one cone (T429R23 and R24, T1102R9 and R10) contain rare brown amphibole and biotite, and benmoreite samples from two different eruptions (T425R1 and R2, T1102R1 to R7) also contain rare brown amphibole microphenocrysts.

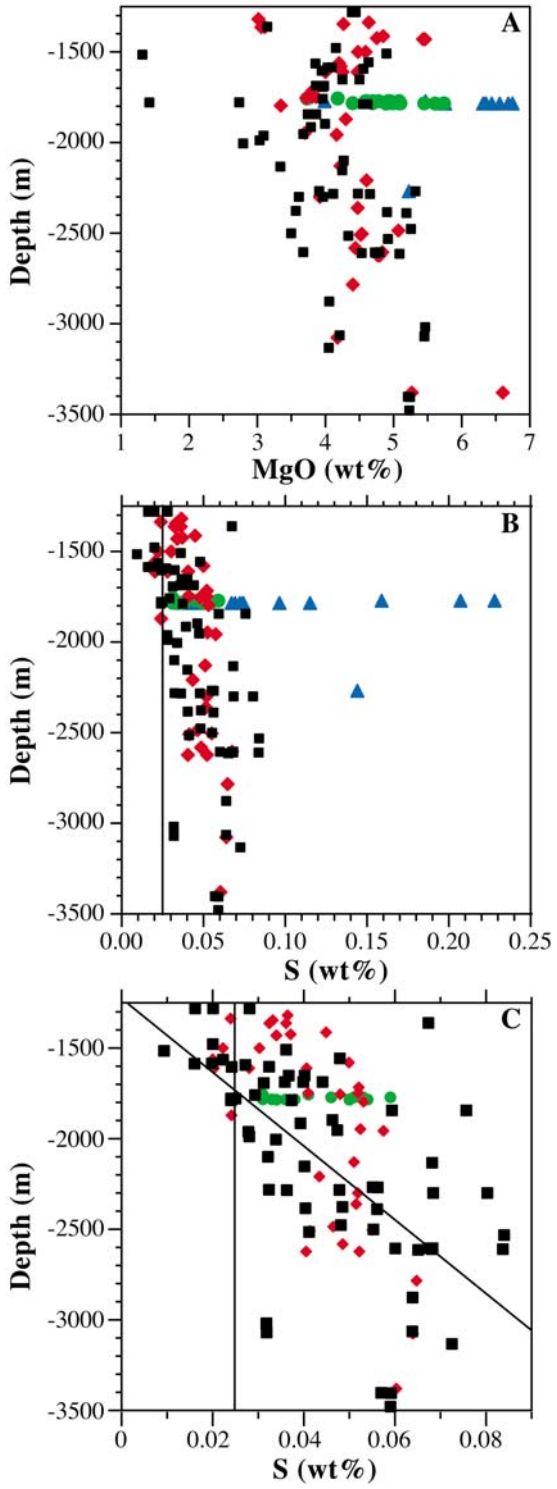

[29] Other mugearite glasses range from nearly aphyric with only small plagioclase laths, to phyric with phenocryst assemblages of olivine, olivine plus plagioclase, to megaphyric or ankaramitic with abundant large clinopyroxene and less abundant olivine. Dredged samples D3–4 and D3–20 [*Davis et al.*, 2002] have glass rinds of mugearite composition, similar ankaramite petrography, and their whole-rock analyses indicate they are alkalic basalt. Benmoreite glass can contain abundant plagioclase or be nearly aphyric with only small laths of plagioclase and small clinopyroxene crystals. Trachyandesite is similar in being essentially aphyric to containing plagioclase and rare clinopyroxene. Tephrite is also variable in phenocryst assemblage ranging from aphyric samples to ones with abundant plagioclase, olivine plus clinopyroxene plus plagioclase, rare olivine, or clinopyroxene plus plagioclase.

4.4. Mineral Chemistry

[30] No systematic survey of the mineral compositions of the lavas has been done, although some phenocrysts and microphenocrysts of olivine (48 analyses), clinopyroxene (30 analyses), and plagioclase (75 analyses) are reported by *Davis et al.* [2007, supplemental tables]. Olivine ranges from $Fo_{87.2}$ to $Fo_{79.3}$ and have NiO as high as 0.28 wt % with the more forsteritic crystals in alkalic basalt and the less forsteritic ones in mugearite. Plagioclase ranges from $An_{68.5}Or_{1.7}$ to $An_{29.7}Or_{5.8}$ with the more calcic crystals in alkalic basalt and the least calcic in mugearite. Clinopyroxene ranges from Wo_{45} to $Wo_{52.3}$, $En_{34.8}$ to $En_{46.6}$, and $Fs_{8.2}$ to $Fs_{14.0}$. Cr_2O_3 ranges up to 0.99 wt %, TiO_2 varies from 1.2 to 6.0 wt %, Na_2O from 0.52 to 0.82 wt %, SiO_2 from 50.2 to 42.1 wt %, and Al_2O_3 from 5.0 to 13.1 wt % with most in the 6 to

Figure 9. (a) MgO plotted as a function of depth showing a weak trend of increasing MgO in glasses with increasing depth. (b) S plotted as a function of depth showing high S content of glass inclusions and the low S contents of glass. (c) The same S data plotted without the glass inclusion data showing the trend of higher S with increasing depth. The diagonal line is a linear fit to the data. The vertical line in Figures 9b and 9c is at 0.025 wt % S and denotes the approximate maximum concentration of S in subaerial Hawaiian basalt. Symbols as in Figure 6.

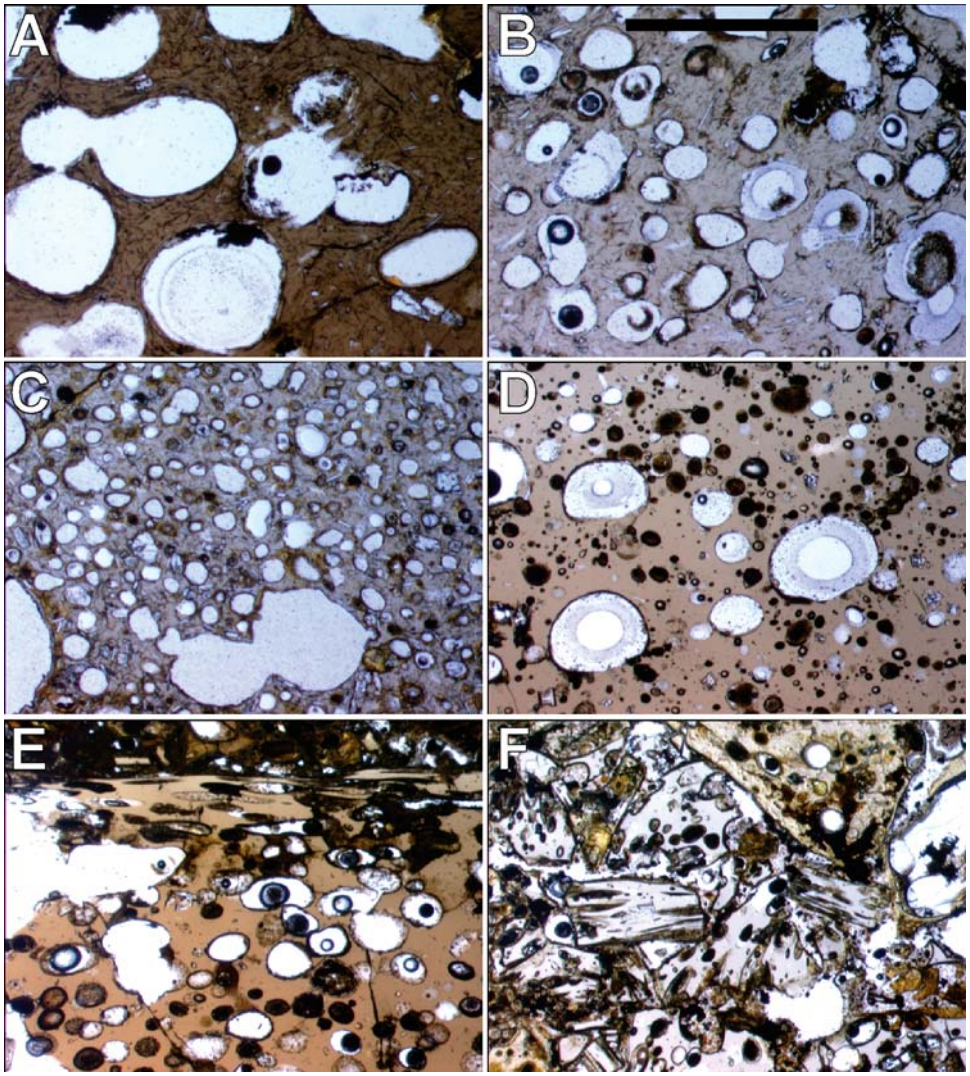

Figure 10. Photomicrographs showing vesicle shape and size distributions. Scale is the same in all images with bar equal to 1 mm. (a) Lava rind sample T140R7 showing large (0.5–1 mm) vesicles that are coalesced into a few dumbbell-shaped vesicles. (b) Lava rind of sample T140R10 showing mostly coalesced larger (0.3–0.4 mm) spherical vesicles. (c) Glass gravel fragment from gravity core SMT07GC6 showing abundant 0.1–0.2 mm nearly spherical vesicles and a few larger coalesced, dumbbell-shaped vesicles as large as 2 mm. (d) Volcaniclastite T147R16 showing a large variation in slightly ovoid vesicle sizes up to about 0.4 mm. (e) Volcaniclastite T427R2 showing a varied population of spherical vesicles inside the clast and stretched bubbles at the edge of the clast. (f) Volcaniclastite sample T428R14 showing stretched vesicles or small spherical vesicles in side-by-side shards.

8 wt % range. Many of these analyses are from dredged samples described by *Davis et al.* [2002] rather than from these ROV-collected samples. New mineral chemistry of the olivine and clinopyroxene phenocrysts that contain the analyzed glass inclusions are presented in Data Set S2. The clinopyroxene host phases are of diopside to salite composition and fall within the range of compositions outlined above, although toward the low end in TiO_2 and Fs component. They most likely weathered out of volcaniclastic deposits of ankaramite. The sole analyzed olivine, from a tephrite sample in SO7GC3, is more iron-rich at $Fo_{75.6}$ than any previously analyzed olivine.

5. Discussion

5.1. Duration of Seamount Construction

[31] The seamount is constructed of numerous volcanic cones seen in the bathymetric data. These cones appear to be monogenetic as our analyses of multiple samples from the same cone are always similar to one another. The age data from Davidson

document about 5 Ma of volcanic activity (from 14.8 to 9.8 Ma) during which very similar alkalic lavas erupted. In contrast, most oceanic volcanoes grow rapidly and have rather brief life spans. For example, the enormous volcanoes that make up the Hawaiian Islands are generally thought to grow in roughly 1 to perhaps 1.5 Ma [*Moore and Clague*, 1992; *DePaolo and Stolper*, 1996], with minor strongly alkalic rejuvenated stage eruptions that can occur as long as a few Ma later (see summary by *Clague and Dalrymple* [1987]). Near-ridge seamounts such as the Vance, President Jackson, and Taney Seamounts offshore western North America are also thought to grow very rapidly. *Clague et al.* [2000] proposed that they grew in <100 ka. Few submarine volcanoes have had enough samples dated to reliably assess how long they took to grow. An exception is Jasper Seamount offshore Baja California where *Pringle et al.* [1991] dated 9 samples from three chemically distinct lava series that erupted over about 6 Ma, although the younger rock series may be equivalent to rejuvenated stage lavas in Hawaii [*Gee et al.*, 1991; *Konter et al.*, 2009]. Other ocean islands, particularly in the Atlantic Ocean, are known to have long eruptive histories spanning millions of years, but at most, lava compositions vary through that history, much like in Hawaii.

[32] We conclude that Davidson Seamount, and other structurally similar volcanoes along the west coast of North America south of San Francisco [*Davis et al.*, 2002, also manuscript in preparation, 2009] and as far south as Guadalupe Island [*Batiza*, 1977] and Sara, Rosana, Rosa, and Nithya seamounts offshore Baja California [*Tian et al.*, 2008], have similar origins. Some of them, such as Davidson and San Juan have unusual long eruptive histories: 5 Ma at Davidson and 9.7 Ma at San Juan (Davis et al., manuscript in preparation, 2009). We suspect that Davidson, because of its location atop a spreading center abandoned about 18–20 Ma, actually started to form then and has taken about 8–10 Ma to grow. With a total volume of only 320 km^3, the rate of magma production is only 0.000032 km^3/year over 10 Ma compared with the rate at Kilauea of about 0.08 km^3/yr [*Denlinger*, 1997]. This magma supply rate is only 0.04% that at Kilauea. Since the individual eruptions at Davidson are also small, it is apparent that Davidson erupted infrequently even when it was active.

[33] This infrequency of eruptions was hypothesized by *Davis et al.* [2002] because there was no evidence of collapse structures such as calderas or pit craters that might indicate shallow magma storage inside the volcano. A lack of shallow storage implies that magma supply is so low that such storage chambers cannot be thermally maintained between injections of magma and they crystallize.

[34] We also note that the ages of the lavas bear only a weak relationship to position on the volcano (Figures 3 and 4). Old and young cones occur near the summit, deep on the flanks, and from end to end of the volcano. This random age distribution indicates that each new magma batch was injected into a cool volcano where it found the path of least resistance to reach the surface and erupt.

5.2. Spatial and Time Distribution of Davidson Melts

[35] We have shown that the compositions of the glasses show no strong systematic distribution on the seamount (Figure 8). There is no zoning, as seen at Jasper Seamount [*Gee et al.*, 1991, *Konter et al.*, 2009] with less alkalic melts on the deep flanks and more alkalic melts nearer the summit. There is a very crude zoning with less fractionated (higher MgO) melts more common deeper on the flanks and more fractionated melts (lower MgO) more common nearer the summit (Figure 9a), but a less complete data set than what we have would be unlikely to reveal this relation.

[36] The melt compositions show a systematic change with time with younger lava generally being less fractionated (Figure 5), but the correlation is rough at best. For example, 11 hawaiite samples include the oldest (14.83 Ma) and the youngest (9.77 Ma) samples dated. Three alkalic basalts have almost as large a range (from 10.30 to 14.19 Ma). The most fractionated sample dated, a trachyte, is 14.75 Ma, whereas the next most fractionated sample, a benmoreite, is 11.60 Ma. One could achieve less and less fractionated lavas with time if the eruption frequency increased during the formation of the seamount. However, there is no apparent relation between fractionation and the time between eruptions, although we have only dated a subset of the extant cones on the volcano. The many other cones we sampled yielded only volcaniclastic samples or highly altered lavas with no phase such as plagioclase that could be separated and dated.

[37] The analyzed xenocrystic and xenolithic clinopyroxene and plagioclase are typical of those in

alkalic lavas [*Davis et al.*, 2007] and give no hint of a hidden interior of tholeiitic basalt composition.

5.3. Liquid Line of Descent for Davidson Lavas?

[38] All of the variation diagrams for the glasses (Figure 7) show a wide scatter of compositions at the same MgO content that indicates that these melts are not related by crystal fractionation along a single liquid line of descent [*Davis et al.*, 2007]. There are no obvious inflection points that might indicate when different phases started to crystallize, with the exception of the low TiO_2 observed for the benmoreites and trachytes that indicate crystallization of Fe-Ti oxide, and low P_2O_5 in the trachytes that indicate crystallization of apatite by this advanced stage of fractionation. The lack of a well-defined liquid line of descent is important because the whole-rock data [*Davis et al.*, 2002; Castillo et al., submitted manuscript, 2009] show these same scattered trends, but it is unclear if the scatter could simply reflect variable amounts of phenocrysts and xenocrysts [*Davis et al.*, 2007]. The glass data demonstrate that this is indeed a feature of the melts that requires varying degrees of partial melting, in addition to varying amounts of crystal fractionation. The glass inclusion data have not been included in our analysis of interelement trends since inclusions can be modified by reequilibration with their host crystals.

[39] Lavas from one cone (T147R8 and T147R9) are unique in having common amphibole as a microphenocryst phase, suggesting that different melts also contain different volatile abundances. The high water content implied by the presence of amphibole is apparently related to degree of melting since this one lava plots on the boundary between hawaiite and tephrite and is the most alkaline, or smallest percent partial melt, glass recovered from Davidson.

[40] Calculations on these compositions [*Davis et al.*, 2007] using MELTS program [*Ghiorso and Sack*, 1995] suggest that the SiO_2 and Al_2O_3 enrichment observed in the trachytic melts cannot be achieved at the 0.7–0.9 GPa required by the amount of clinopyroxene fractionation needed to reduce CaO/Al_2O_3 as observed. The SiO_2 enrichment in trachyte appears to require low pressure (0.1–0.3 GPa). In addition, no combination of pressure and water content led to amphibole as a crystallizing phase. The detailed petrogenesis of the lavas has been discussed at length by *Davis et al.* [2002, 2007] and Castillo et al. (submitted manuscript, 2009) and is beyond the scope of this paper.

5.4. Volatile Exsolution Prior to and During Eruption

[41] The S content of the melts can be estimated from the S content of glass inclusions trapped in mineral phases. The highest concentrations are about 0.21 wt % S. None of the glasses contain nearly this much S and we infer that they have lost some of their S during vesiculation and bubble escape [*Dixon et al.*, 1997]. The glass analyses indicate losses of 60% to 95% of initial S. There is a strong correlation of decreasing S with decreasing depth (Figures 9b and 9c) and the glasses from the shallowest depths have S concentrations that overlap with the S concentrations commonly found in subaerial basalts from Hawaii [*Moore and Clague*, 1987]. However, we see little other evidence to support the idea that Davidson was once an island [*Paduan et al.*, 2009] and conclude that these fractionated alkalic lavas had high volatile contents that caused extensive vesiculation (Figure 10) and volatile loss, under shallow to deep submarine conditions. Other alkalic lavas erupted submarine at the North Arch [*Dixon et al.*, 1997] and Loihi Seamount [*Dixon and Clague*, 2001] have lost up to ~50% of their initial S during magma degassing, at depths as shallow as 1050 m on Loihi or 3900–4380 m deep in the North Arch.

[42] If we assume that the summit of Davidson reached to within less than 100 m of sea level when the summit cone formed at 14.8 Ma, then the average subsidence rate has been about 0.08 mm/yr, comparable to the subsidence rate on young ocean crust [*Stein and Stein*, 1993], but far lower than the 2.4 mm/yr determined for Hawaii [*Moore and Clague*, 1992].

[43] The range of S contents in the population of glass inclusions shows that S loss during vesiculation was already taking place as these magmas crystallized and formed the host phenocrysts. *Davis et al.* [2002, 2007] have argued that the magmas were stored near the base of the lithosphere, where they cooled and crystallized, and apparently lost some of their volatile component, prior to migrating through the crust where they also acquired a diverse assemblage of xenoliths and xenocrysts. Their final rise to eruption, powered by the high volatile content and abundant vesicles (only some of which escaped from the melt) was rapid enough that the magmas could carry some small ultramafic mantle xenoliths in suspension.

These magmas erupted to form common deposits of volcaniclastic rocks, many containing highly vesicular (Figure 10) clasts of scoria [*Davis and Clague*, 2003].

6. Conclusions

[44] Two-hundred and eighty-six rock samples of lava, volcaniclastite, and erratics from the continental margin were collected from Davidson Seamount during 27 ROV *Tiburon* dives, in addition to clastic glass fragments from one push core and 4 gravity cores. The 99 glass analyses are of hawaiite (62%), mugearite (13%), alkalic basalt (9%), and tephrite (8%), with minor transitional basalt (2%), benmoreite (2%), and trachyandesite (2%). The lithologies are nearly randomly distributed in both space and time, with a subtle tendency for the shallow lavas to be more fractionated. The volcano was constructed on crust inferred to be 20 Ma from seafloor magnetic anomalies. Ar-Ar incremental heating age data for 20 of the samples range from 9.8 to 14.8 Ma. The composition of the 18 reliably dated volcanic cones varies with age such that the oldest lavas are the most fractionated. The numerous small cones of disparate chemistry and the long eruptive period suggest episodic growth of the volcano over at least 5, and perhaps as long as 10 million years if it began to grow when the spreading ridge was abandoned. The magmas were stored, cooled, crystallized and began to degas near the base of the lithosphere before rising rapidly due to their high bubble content. Many of the eruptions included a pyroclastic component that produced abundant volcaniclastic rocks with highly vesicular clasts of scoria.

Acknowledgments

[45] We wish to thank the captain and crew of the R/V *Western Flyer* and the ROV *Tiburon* pilots. We also thank NOAA's Sanctuary Program, the BBC, and Tessa Hill for including our work during their dives to Davidson. Mike McCann assisted in reconstructing the navigation for the 2000 dives and dive T425. D.A.C., A.S.D., and J.B.P. were supported by the Monterey Bay Aquarium Research Institute through a grant from the David and Lucile Packard Foundation. P.C. and P.L. were supported by a grant from NOAA's West Coast NURP Office, and A.P.D. was supported by NOAA's MBNMS and grants from the Ocean Exploration Program.

References

Andrews, A. H., G. M. Cailliet, L. A. Kerr, K. H. Coale, C. Lunstrom, and A. P. DeVogelaere (2005), Investigations of age and growth for three deep-sea corals from the Davidson Seamount off central California, in *Cold-Water Corals and Ecosystems*, edited by A. Freiwald and J. M. Roberts, pp. 1021–1038, Springer, Berlin.

Atwater, T., and J. Severinghaus (1989), Tectonic maps of the northeast Pacific, in *The Eastern Pacific Ocean and Hawaii*, edited by E. L. Winterer, D. M. Hussong, and R. W. Decker, pp. 15–20, Geol. Soc. of Am., Boulder, Colo.

Batiza, R. (1977), Petrology and geochemistry of Guadalupe Island: An alkalic seamount on a fossil ridge crest, *Geology*, *5*, 760–764, doi:10.1130/0091-7613(1977)5<760:PACOGI>2.0.CO;2.

Bohrson, W. A., M. R. Reid, A. L. Grunder, M. T. Heizler, T. M. Harrison, and J. Lee (1996), Prolonged history of silicic peralkaline volcanism in the eastern Pacific Ocean, *J. Geophys. Res.*, *101*, 11,457–11,474.

Choe, W. H., J. I. Lee, M. J. Lee, S. D. Hur, and Y. K. Jin (2007), Origin of E-MORB in a fossil spreading center: The Antarctic-Phoenix Ridge, Drake Passage, Antarctica, *Geosci. J.*, *11*, 185–199, doi:10.1007/BF02913932.

Choi, S.-H., W.-H. Choe, and J.-I. Lee (2008), Mantle heterogeneity beneath the Antarctic-Phoenix Ridge off Antarctic Peninsula, *Isl. Arc*, *17*, 172–182.

Clague, D. A., and G. B. Dalrymple (1987), The Hawaiian-Emperor volcanic chain: Part I. Geologic evolution, *U.S. Geol. Surv. Prof. Pap.*, *1350*, chap. 1, part 1, 5–54.

Clague, D. A., J. R. Reynolds, and A. S. Davis (2000), Near-ridge seamount chains in the northeastern Pacific Ocean, *J. Geophys. Res.*, *105*, 16,541–16,561, doi:10.1029/2000JB900082.

Cox, K. G., J. D. Bell, and R. J. Pankhurst (1979), *The Interpretation of Igneous Rocks*, 450 pp., Allen and Unwin, London.

Davis, A. S., and D. A. Clague (2003), Hyaloclastite from Miocene seamounts offshore central California: Compositions, eruption styles, and depositional processes, in *Explosive Subaqueous Volcanism*, *Geophys. Monogr. Ser.*, vol. 140, edited by J. D. L. White, J. L. Smellie, and D. A. Clague, pp. 129–142, AGU, Washington, D. C.

Davis, A. S., D. A. Clague, and W. F. Friesen (1994), Petrology and mineral chemistry of basalt from Escanaba Trough, southern Gorda Ridge, *U.S. Geol. Surv. Bull.*, *2022*, 153–170.

Davis, A. S., S. H. Gunn, W. A. Bohrson, L. B. Gray, and J. R. Hein (1995), Chemically diverse, sporadic volcanism at seamounts offshore southern and Baja California, *Geol. Soc. Am. Bull.*, *107*, 554–570, doi:10.1130/0016-7606(1995)107<0554:CDSVAS>2.3.CO;2.

Davis, A. S., D. A. Clague, W. A. Bohrson, G. B. Dalrymple, and H. G. Greene (2002), Seamounts at the continental margin of California: A different kind of oceanic intraplate volcanism, *Geol. Soc. Am. Bull.*, *114*, 316–333, doi:10.1130/0016-7606(2002)114<0316:SATCMO>2.0.CO;2.

Davis, A. S., D. A. Clague, and J. B. Paduan (2007), Diverse origins of xenoliths from seamounts at the continental margin, offshore central California, *J. Petrol.*, *48*, 829–852, doi:10.1093/petrology/egm003.

Denlinger, R. (1997), A dynamic balance between magma supply and eruption rate at Kilauea Volcano, Hawaii, *J. Geophys. Res.*, *102*, 18,091–18,100, doi:10.1029/97JB01071.

DePaolo, D. J., and E. M. Stolper (1996), Models of Hawaiian volcano growth and plume structure: Implications of results from the Hawaii Scientific Drilling Project, *J. Geophys. Res.*, *101*, 11,643–11,654, doi:10.1029/96JB00070.

DeVogelaere, A. P., E. J. Burton, T. Trejo, D. A. Clague, M. N. Tamburri, G. M. Cailliet, R. E. Kochevar, and W. J. Douros (2005), Deep sea corals and resource protection at the

Davidson Seamount, California, U.S.A., in *Cold-Water Corals and Ecosystems*, edited by A. Freiwald and J. M. Roberts, pp. 1189–1198, Springer, Berlin.

Dixon, J. E., and D. A. Clague (2001), Volatiles in basaltic glass from Loihi Seamount, Hawaii: Evidence for a relatively dry plume component, *J. Petrol.*, *42*, 627–654, doi:10.1093/petrology/42.3.627.

Dixon, J. E., D. A. Clague, P. Wallace, and R. Poreda (1997), Volatiles in alkalic basalts from the North Arch Volcanic Field, Hawaii: Extensive degassing of deep submarine-erupted alkalic series lavas, *J. Petrol.*, *38*, 911–939, doi:10.1093/petrology/38.7.911.

Duncan, R. A., and R. A. Keller (2004), Radiometric ages for basement rocks from the Emperor Seamounts, ODP Leg 197, *Geochem. Geophys. Geosyst.*, *5*, Q08L03, doi:10.1029/2004GC000704.

Gee, J., H. Staudigel, and J. H. Natland (1991), Geology and petrology of Jasper Seamount, *J. Geophys. Res.*, *96*, 4083–4105, doi:10.1029/90JB02364.

Ghiorso, M. S., and R. O. Sack (1995), Chemical mass transfer in magmatic processes IV: A revised and internally consistent thermodynamic model for the interpolation and extrapolation of liquid-solid equilibria in magmatic systems at elevated temperatures and pressures, *Contrib. Mineral. Petrol.*, *119*, 197–212, doi:10.1007/BF00307281.

Konter, J., H. Staudigel, J. Blichert-Toft, B. B. Hanan, M. Polve, G. R. Davies, N. Shimizu, and P. Schiffman (2009), Geochemical stages at Jasper Seamount and the origin of intraplate volcanoes, *Geochem. Geophys. Geosyst.*, *10*, Q02001, doi:10.1029/2008GC002236.

Koppers, A. A. P. (2002), ArArCALC—Software for $^{40}Ar/^{39}Ar$ age calculations, *Comput. Geosci.*, *28*, 605–619, doi:10.1016/S0098-3004(01)00095-4.

Koppers, A. A. P., H. Staudigel, and J. R. Wijbrans (2000), Dating crystalline groundmass separates of altered Cretaceous seamount basalts by the $^{40}Ar/^{39}Ar$ incremental heating technique, *Chem. Geol.*, *166*, 139–158, doi:10.1016/S0009-2541(99)00188-6.

Koppers, A. A. P., H. Staudigel, and R. A. Duncan (2003), High-resolution $^{40}Ar/^{39}Ar$ dating of the oldest oceanic basement basalts in the western Pacific basin, *Geochem. Geophys. Geosyst.*, *4*(11), 8914, doi:10.1029/2003GC000574.

Lonsdale, P. (1991), Structural patterns of the Pacific floor offshore of peninsular California, in *The Gulf and Peninsular Provinces of the Californias*, edited by J. P. Dauphin and B. T. Simoneit, *AAPG Mem.*, *47*, 87–125.

Lundsten, L., J. P. Barry, G. M. Cailliet, D. A. Clague, A. P. DeVogelaere, and J. B. Geller (2009a), Benthic invertebrate communities on three seamounts off southern and central California, USA, *Mar. Ecol. Prog. Ser.*, *374*, 23–32, doi:10.3354/meps07745.

Lundsten, L., C. R. McClain, J. P. Barry, G. M. Cailliet, D. A. Clague, and A. P. DeVogeleare (2009b), Ichthyfauna on three seamounts off southern and central California, USA, *Mar. Ecol. Prog. Ser.*, *389*, 223–232.

MBARI Mapping Team (2001), West Coast seamounts and ridges multibeam survey, *MBARI Digital Data Ser.*, *7*, Moss Landing, Calif.

Moore, J. G., and D. A. Clague (1987), Coastal lava flows from Mauna Loa and Hualalai Volcanoes, Kona, Hawaii, *Bull. Volcanol.*, *49*, 752–764, doi:10.1007/BF01079826.

Moore, J. G., and D. A. Clague (1992), Volcano growth and evolution of the island of Hawaii, *Geol. Soc. Am. Bull.*, *104*, 1471–1484, doi:10.1130/0016-7606(1992)104<1471:VGAEOT>2.3.CO;2.

Paduan, J. B., D. A. Clague, and A. S. Davis (2007), Erratic continental rocks on volcanic seamounts off the US west coast, *Mar. Geol.*, *246*, 1–8, doi:10.1016/j.margeo.2007.07.007.

Paduan, J. B., D. A. Clague, and A. S. Davis (2009), Evidence that three seamounts off Southern California were ancient islands, *Mar. Geol.*, *265*, 146–156.

Pringle, M. S., H. Staudigel, and J. Gee (1991), Geochronology of Jasper Seamount: Seven million years of volcanism, *Geology*, *19*, 364–368, doi:10.1130/0091-7613(1991)019<0364:JSSMYO>2.3.CO;2.

Renne, P. R., C. C. Swisher, A. L. Deino, D. B. Karner, T. L. Owens, and D. J. DePaolo (1998), Intercalibration of standards, absolute ages and uncertainties in $^{40}Ar/^{39}Ar$ dating, *Chem. Geol.*, *145*, 117–152, doi:10.1016/S0009-2541(97)00159-9.

Stein, C. A., and S. Stein (1993), Constraints on Pacific midplate swells from global depth-age and heat flow-age models, in *The Mesozoic Pacific: Geology, Tectonics, and Volcanism*, *Geophys. Monogr. Ser.*, vol. 77, edited by M. S. Pringle et al., pp. 53–76, AGU, Washington, D. C.

Tian, L., P. R. Castillo, and P. F. Lonsdale (2008), Petrology and geochemistry of abandoned spreading center lavas off Baja California: Implications for intraplate magmatism in eastern Pacific, *Eos Trans. AGU*, *89*(52), Fall Meet. Suppl., Abstract V43B-2158.